J Nanopart Res (2011) 13:3033–3042
DOI 10.1007/s11051-010-0200-3

RESEARCH PAPER

Effect of milling time and heat treatment on the composition of $CuIn_{0.75}Ga_{0.25}Se_2$ nanoparticle precursors and films

B. Vidhya · S. Velumani · R. Asomoza

Received: 7 May 2010 / Accepted: 20 December 2010 / Published online: 6 March 2011
© Springer Science+Business Media B.V. 2011

Abstract Preparation of pure phase $CuIn_{0.75}Ga_{0.25}Se_2$ nanoparticle powder by ball milling technique has been confirmed for the milling time of more than 45 min at 1200 rpm. Formation of shear bands responsible for breakdown of grains and generation of nanostructure during mechanical alloying, dislocation and defects induced due to milling has been studied by High-Resolution Transmission Electron Microscopy (HRTEM) analysis. Deviation in final composition of the products from those of starting materials has been discussed based on low volatilization of Se. Effect of milling time on the phase formation, particle size, and composition has been discussed in detail. Decrease in grain size from 12.44 to 7.96 nm has been observed with the increase in milling time. Mechanically induced self-propagating reaction mechanism which occurred during milling process is also discussed. Nanoparticle precursor was mixed with organic binder material for rheology of mixture to be adjusted for screen printing, and the films are subjected to heat treatment at five different temperatures in nitrogen ambient for 25 min. Average grain size calculated by Scherrer's formula was almost the same irrespective of temperature. Reproducibility of precursor composition in the deposited films has been discussed in detail.

Keywords CIGS · Ball milling · EDX · HRTEM · Synthesis

B. Vidhya (✉) · S. Velumani · R. Asomoza
Department of Electrical Engineering (SEES), CINVESTAV, 07360 Mexico, D.F., Mexico
e-mail: vidhyabhojan@gmail.com

S. Velumani
e-mail: velu@cinvestav.mx

S. Velumani
Nanoscience and Nanotechnology Programme, CINVESTAV, 07360 Mexico, D.F., Mexico

Introduction

The energy conversion efficiency of $CuInGaSe_2$ (CIGS) has reached 19.5% (692 mV, 35.2 mA/cm^2, FF 79.9%) at NREL (Contreras et al. 2006). However, laboratory scale efficiency is still lower than that of the expected theoretical calculation efficiency (30%) (Choi and Lee 2007). In last few years, researchers tried to use semiconductor nanocrystals in solar cells technology. They have demonstrated that the performance of photovoltaic cells may be improved using nano structured materials synthesis and device fabrication (Lin et al. 2008). For this reason, CIGS nanoparticles have been studied by several authors. Commonly used methods for synthesis of CIGS nanoparticles include solvothermal technique and low temperature colloidal synthesis (Luo et al. 2010a, b; Ahn et al. 2007; Suryanarayana et al. 2001). Among them, solvothermal technique is time consuming, for example, a reaction temperature of

280 °C for 36 h and then cooling to room temperature has been reported (Chun et al. 2005). Low temperature colloidal synthesis uses Na_2Se as one of the starting materials, which is highly toxic (Ahn et al. 2007). Even though there is a recent report on CIS films prepared by combustion method and spin-coating process (Luo et al. 2010a, b), there is no such reports on CIGS. Addition of Ga precursor could make this process difficult, due to the low melting temperature of Ga. Thus, mechanochemical synthesis is considered as a suitable method which employs the elemental (Cu, In, Ga, and Se) sources and a comparatively less time (Suryanarayana et al. 2001). Recently, a wide variety of nanoparticles have been synthesized by mechanochemical technique, including CdO, GaN, ZnO, TiO_2, CIGS, etc.(Yang et al. 2004; Cai et al. 2002; Dodd et al. 2008; Gesenhues 1999; Vidhya et al. 2010).

One of the special qualities of CIGS is its variable band gap, which increases from 1.02 to 1.66 eV by increasing the Ga/(Ga + In) ratio from 0 to 1 (Lundberg et al. 2003). Also CIGS films should have Cu/(In + Ga) < 1, i.e., Cu poor and In + Ga rich, which would create an abundance of Cu vacancies at the CIGS/CdS interface. The ionic radii of Cu (0.070 nm) and Cd (0.097 nm) are very close, and the substitution of Cd in Cu vacancy sites is most likely, and therefore the resulting composition mixing will reduce the effects of interface (CdS/CIGS) carrier recombination, thus leading to higher efficiency. Apart from this effect, Sakurai et al. (2003) have reported that Cu/(In + Ga) affect the morphology of CIGS absorber layer. Similarly, Kaufamn et al. (2005) have observed an increase in roughness of film when Cu/(In + Ga) > 1. Also in our previous report we have confirmed that the relative Ga composition x = Ga/(In + Ga) affects the structural characteristics of ball milled CIGS precursor powder (Vidhya et al. 2010). Based on above aspects, the optimum value of Cu/(In + Ga) ranges from 0.8 to 0.95, which is less than 1 (Chityuttakan et al. 2006; Nouiri et al. 2007; Contreras et al. 2005) thus the composition of precursor powder and film plays a significant role in cell efficiency.

Recently, Benslim et al. (2010) have reported the mechanochemical synthesis of $CuIn_{0.5}Ga_{0.5}Se_2$ nanoparticles of size 16.4 ± 0.2 nm with Cu-rich composition, but effect of milling time on composition of CIGS nanoparticles has not been reported till date. In this article, we have discussed this aspect in detail, showing the difference in composition based on low volatilization of Se. It has been reported that in the process using $CuIn_xGa_{1-x}Se_2$ nanoparticle precursors the composition control of precursor and final product film is easy because the composition of precursor nanoparticle is transferred directly to that of as-coated and selenized film without change in the atomic ratio of elements (Panthani et al. 2008). This can be coupled with the ability to coat a large area with excellent control of composition, laterally in that any part of the films has same composition as that of precursor nanoparticles. To the best of our knowledge, there are no reports justifying the transfer of precursor nanoparticle composition directly on film deposited by screen printing followed by heat treatment. Therefore, in this study, we have discussed in detail the possibility of reproducing the precursor composition in deposited nanoparticle films and change in composition due to thermodynamically unstable nature of nanoparticles.

Experimental

Experimental section consists of three parts which include the preparation of $CuIn_{0.75}G_{0.25}Se_2$ nanoparticle precursors followed by screen printing and then characterization of the prepared precursors and films.

Preparation of $CuIn_{0.75}G_{0.25}Se_2$ nanoparticle precursors

i. In the preparation of $CuIn_{0.75}Ga_{0.25}Se_2$ nanoparticle powders, copper granules (>99.9% pure), selenium and indium powders (>99.9% pure), and fine chips/granules of gallium were weighed to correspond to the stoichiometry of $CuIn_{0.75}Ga_{0.25}Se_2$.
ii. This blended elemental mixture and stainless steel balls were loaded in a stainless steel container inside an argon-filled glove box.
iii. Ball-to-powder weight ratio (BPR) was maintained at 5:1. Milling was conducted using a SPEX-8000 mixer/mill at 1200 rpm.
iv. Reactants (Cu, In, Ga, and Se) are initiated by mechanical energy such as collision and friction with the stainless steel balls.
v. The explosive reaction ends in a short time (1 min or less for $CuInSe_2$) (Wada and Kinoshita 2005) this reaction is a type of chain reaction.

vi. After the reaction is completed, synthesized $CuIn_{0.75}Ga_{0.25}Se_2$ powder is pulverized by milling, leading to the formation of nanoparticles.

Deposition of films by screen printing

$CuIn_{0.75}Ga_{0.25}Se_2$ nano particle powder prepared by ball milling is mixed with an organic binder such as ethyl cellulose in the ratio 5:1 followed by the addition of ethylene glycol and ethyl alcohol in the ratio 1:5, which is mixed thoroughly until a semi paste like ink is obtained. This precursor is used for screen printing on glass substrates, which is then subjected to heat treatment for 25 min in nitrogen ambient for different temperatures of 300, 325, 350, 375, and 400 °C.

Characterization techniques

Structure of the prepared nanoparticles and screen printed films were analyzed using an X-ray diffractometer (Siemens D5000, using Cu-Kα radiation with $\lambda = 1.5406$ Å). Measurements were made for 2θ values over 20°–80°. Morphology of the deposited films has been analyzed by JEOL 840 SEM. Particle size of the prepared powders was analyzed by HRTEM JEOL JEM-2010 FEG instrument with a point resolution of 1.9 Å. Samples were placed on carbon copper grid of 300 mesh. The measurements of lattice-fringe spacing and angles recorded in digital high-resolution electron micrographs were made using digital image analysis of reciprocal space parameters. This analysis was carried out with the aid of Digital Micrograph software, Simula TEM. Composition of the nanoparticle and film was analyzed by JEOL 840 SEM-energy dispersive X-ray analysis (EDS).

Results and discussions

Characterization of $CuIn_{0.75}Ga_{0.25}Se_2$ nanoparticles

In this study, $CuIn_{0.75}Ga_{0.25}Se_2$ nanoparticles have been prepared by a simple, low cost mechanochemical synthesis. This process is a dry milling technique in which elemental Cu, In, Ga, and Se are repeatedly welded, fractured, and rewelded under a highly energetic ball charge to prepare $CuIn_{0.75}Ga_{0.25}Se_2$ powders

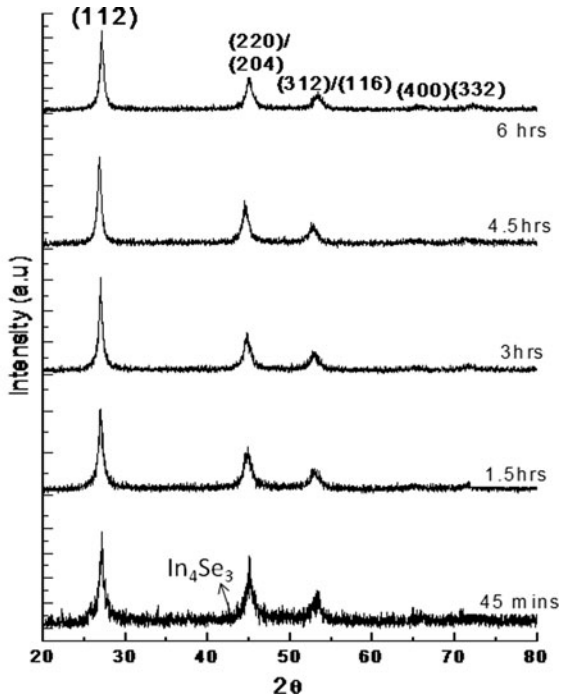

Fig. 1 XRD pattern of ball milled $CuIn_{0.75}Ga_{0.25}Se_2$ nanoparticles

at various milling times of 45 min, 1.5, 3, 4.5, and 6 h. Figure 1 shows the evolution of X-ray diffractograms as a function of milling time, and it is observed that $CuIn_{0.75}Ga_{0.25}Se_2$ phase formation occurs after 45 min of milling. For 45 min milled sample, apart from XRD reflections corresponding to $CuIn_{0.75}Ga_{0.25}Se_2$ chalcopyrite structure an additional reflection at $2\theta = 42.54°$ is also observed which corresponds to In_4Se_3 phase (ICSD #:023465). As milling time progresses, only pure $CuIn_{0.75}Ga_{0.25}Se_2$ phase has been observed, and no phase change has been detected. We can say that the phase formation has occurred very quickly, and increase in milling duration leads to homogenization (Sherif El-Eskandarany et al. 2003). XRD reflections are slightly left shifted with the increase in milling time; this is attributed to the internal stresses induced by milling. These internal stresses modify the lattice parameter and consequently produce an angular shift of XRD peak. This shift is well defined for 3 h of milling and increases continuously with milling time. Similar shift due to the increase in milling time has been observed for $Fe_{50}Ni_{50}$ nanoparticles (Djekoun et al. 2006).

Chalcopyrite structure of $CuIn_{0.75}Ga_{0.25}Se_2$ has been simulated using space group I42d (122) with

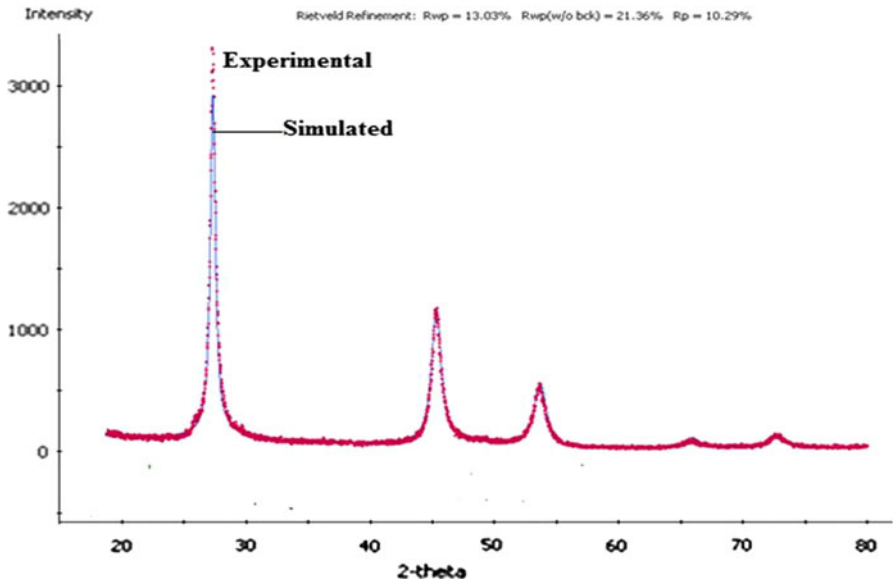

Fig. 2 Simulated and experimental XRD pattern of $CuIn_{0.75}Ga_{0.25}Se_2$ milled for 1.5 h

standard lattice constants $a = 5.673$ Å and $c = 11.322$ Å (JCPDS-40-1488) (Suri et al. 1989), and the experimental diffraction pattern of 1.5 h milled sample is matched with the simulated pattern by Rietveld refinement, as shown in Fig. 2. Here, it should be noted that recent report on 300 rpm ball milled $CuIn_{0.5}Ga_{0.5}Se_2$ showed the presence of In_3Se_4 reflection for 30, 60, and 120 min milling. Therefore, they have achieved the best refinement of XRD patterns by introducing an additional binary phase (InSe) (Benslim et al. 2010). In this study, best refinement is obtained with the single phase $CuIn_{0.75}Ga_{0.25}Se_2$ without inclusion of any binary phases. Hence, we confirm the preparation of pure phase $CuIn_{0.75}Ga_{0.25}Se_2$ nanoparticle powder by low cost mehano-chemical synthesis.

Grain size and lattice constants are determined using Eqs. 1 and 2 and given in Table 1.

$$D = (0.94\lambda)/(\beta\cos\theta) \quad (1)$$

$$1/d^2 = \left(h^2 + k^2\right)/a^2 + l^2/c^2 \quad (2)$$

It is observed that the grain size decreased from 12.44 to 7.96 nm with the increase in milling time from 45 min to 6 h. The prepared nanoparticles did not show any preferred orientation, which is confirmed by nearly equal texture coefficient value calculated using Eq. 3 and given in Table 2.

$$\text{Texture coefficient} = I_{(hkl)}/I_{0(hkl)}\left[1/n \sum_{(i=1\ \text{to}\ n)} I_{(hkl)}/I_{0(hkl)}\right]^{-1} \quad (3)$$

where $I_{(hkl)}$ is the experimental value obtained, $I_{0(hkl)}$ corresponds to standard data, and n is the number of peaks considered.

Table 1 Structural parameters of ball milled $CuIn_{0.75}Ga_{0.25}Se_2$ nanoparticles

Milling time	Grain size D (nm)	a (Å)	c (Å)	c/a	$u = 2 - c/a$
45 min	12.44	5.70	11.32	1.985	0.015
1.5 h	12.24	5.70	11.49	2.015	−0.015
3 h	11.23	5.73	11.43	1.994	0.006
4.5 h	9.94	5.75	11.49	1.998	0.002
6 h	7.96	5.69	11.34	1.992	0.008

Table 2 Calculated texture coefficients of ball milled $CuIn_{0.75}Ga_{0.25}Se_2$ nanoparticles

(*hkl*): Milling time	(112)	(220)/(204)	(312)/(116)
45 min	0.783	1.274	0.803
1.5 h	0.961	1.194	0.833
3 h	1.046	1.119	0.837
4.5 h	1.079	1.082	0.844
6 h	1.092	1.104	0.803

The HRTEM images allow the determination of size of nanoparticles and also the possible induced morphologies, so we used it to recognize these variables from our samples. In Fig. 3a, a single particle is clearly identified with the size of 11.73 nm; this confirms the value of 12.24 nm for 1.5 h milled sample obtained from Scherrer's formula. HRTEM images allow finding defects in the nanocrystalline material as marked with an arrow in Fig. 3a; these can be representatives of the processes that induce the reduction of nanocrystal size during mechanochemical synthesis and thus producing more stress leading to change in lattice parameters and hence the shift in XRD peak as stated above. Figure 3b gives the lattice spacing of 1.72 Å, which corresponds to (116)/(312) planes, we have simulated the crystal planes of $CuIn_{0.75}Ga_{0.25}Se_2$ chalcopyrite structure and matched it with the HRTEM pattern.

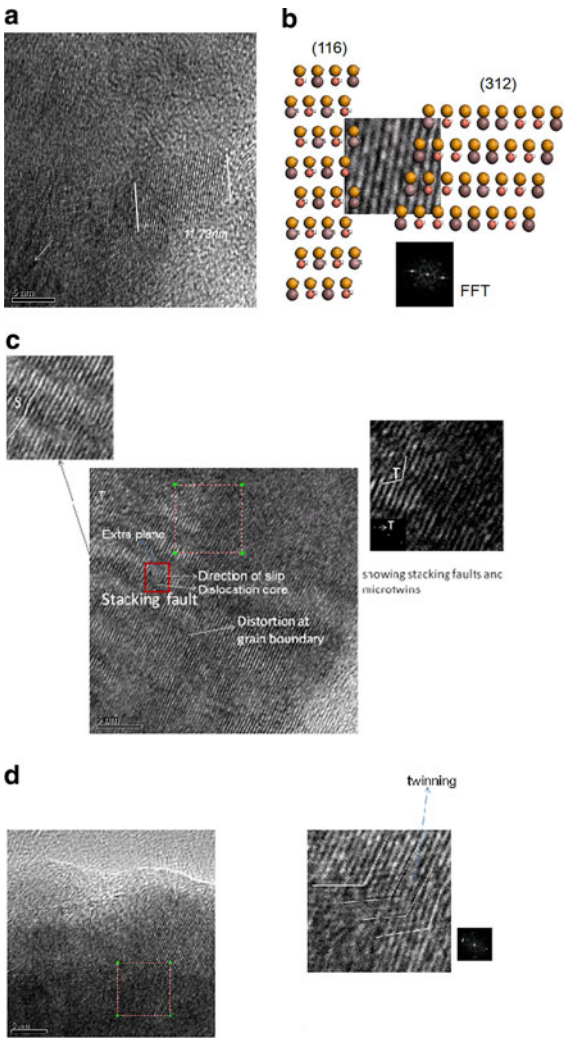

Fig. 3 **a** Nanoparticle of size 11.73 nm, **b** simulated planes and FFT for the particle in Fig. 3a. **c** Distortions, dislocation, and stacking fault. **d** Tetragonal layered structure having deformed and ruptured lattice planes

The HRTEM also revealed that during the process of ball milling large deformations are introduced, like distorted regions within the sub grains, grain boundary and even across entire grains, moiré, fringes, and stacking faults as shown in Fig. 3c. The distorted regions are generated by an accumulation of dislocations from other regions. This sort of distortion is not commonly observed in coarse-grained materials (Reddy et al. 2008). HRTEM photographs also showed that during milling the grains slide and overlap (stacking faults are seen) and that fragmentation and adhesion of grains is a steady process. Newly formed interfaces between grains are brought into intimate contact by subsequent ball collision forming a composite grain. The presence of an extra plane resulted in slip dislocation leading to the formation of core dislocation as shown in Fig. 3c. The bands shown in the grains in Fig. 3c, have also been observed in other studies (Reddy et al. 2008), and have been identified as shear bands. It has been reported that the formation of these shear bands is responsible for breakdown of the grains and generation of nanostructure during mechanical alloying. Apart from this tetragonal-layered structure having deformed and ruptured planes are identified in Fig. 3d, confirming the crystal structure. A moiré pattern develops when there is a small rotation between the two crystals or when there is a slight difference in lattice constant. It gives a kind of magnified image of the boundary. These patterns are evident in our sample, which shows the interruption of long range order in crystallites.

The EDX composition analysis revealed a small deviation from the initial composition $CuIn_{0.75}Ga_{0.25}Se_2$ as given in Table 3. The sample milled for 45 min showed higher amount of In and Se, this is in accordance with XRD results where In_4Se_3 reflection has been observed for this particular milling time as discussed above. This gives the evidence of initiation and formation of $CuIn_{0.75}Ga_{0.25}Se_2$ compound semiconductor (Benslim et al. 2010). With the increase in milling time, increase in percentage of copper and decrease in selenium have been observed, which is in accordance with the results reported by

Table 3 EDX: composition analysis of ball milled $CuIn_{0.75}Ga_{0.25}Se_2$ nanoparticles

Milling time	At% Cu	At% In	At% Ga	At% Se	Cu/(In + Ga)	Ga/(In + Ga)
45 min	12.89	24.10	7.14	55.87	0.412	0.228
1.5 h	24.39	21.42	7.22	46.97	0.851	0.252
3 h	27.76	21.07	7.90	43.27	0.958	0.272
4.5 h	31.93	20.19	4.74	43.15	1.280	0.190
6 h	33.49	20.28	5.50	42.31	1.299	0.213

Benslim et al. (2010), higher milling time would have led to loss of Se and/or contamination from the container and balls. Also volatilization of Se could explain the decrease in selenium. Whereas the loss of In and Ga was another condition, as we know, both In and Ga are soft metals so it can stick to the vessel wall easily. The final product was Cu-rich compound with the increase in milling time. Thus, milling time not only influences phase formation and particle size but also affects the composition of final product. From XRD and EDX analysis, the sample milled for 1.5 h with nearly stoichiometric composition $CuIn_{0.75}Ga_{0.25}Se_2$ without any binary phases has been chosen as precursor for screen printing.

Reaction mechanism

It has been reported that a self-propagating high-temperature synthesis SHS reaction requires a minimum adiabatic temperature (T_{ad}) of about 1800 K or $[\Delta H/Cp]_{298\ K} = 2000$ K. The T_{ad} decreased during milling because the reactants were repeatedly welded and fractured throughout mechanochemical process (MCP). As a result, the interfacial area increased, clean interfaces exposed and the defect density increased, which would allow the diffusion along defects. So this minimum T_{ad} was reduced to approximately 1300 K during milling (Shen et al. 2006), Literature values of calculated enthalpy formation for $CuInSe_2$, ΔH_f ($CuInSe_2$) = −218.50 kJ/mol (Jäger-Waldau et al. 1998) and for $CuGaSe_2$, ΔH_f ($CuGaSe_2$) = −251 kJ/mol (Wu et al. 2010). Gmelin and Hönle (1995) had determined the molar heat capacity of $CuInSe_2$, Cp (298.15 K) = 99.82 J/mol K. Therefore, a measure of the adiabatic temperature of reaction, $[\Delta H/Cp]298\ K = 2188.94$ K, which is close to 2000 K and hence the critical value of 1300 K. So CIGS could be synthesized easily by ball milling. The T_{ad} could be obtained by assuming that the heat released by the reaction ultimately was used to raise the temperature of the final products (Virtuani et al. 2006). From thorough literature analysis, the reaction was ignited by mechanical energy. Strong heat released from reaction raised the temperature of the system over the melting point of $CuIn(Ga)Se_2$, which is in between 987 and 1040 °C. Then, reaction proceeded in the mode of self-propagation. CIGS compound was synthesized finally. In addition, heat of vaporization of Se is about 26.3 kJ/mol, which is much smaller than the heat released from reaction. So selenium particles volatilized easily during MCP leading to loss of Se with the increase in milling time as discussed above.

Characterization of screen printed $CuIn_{0.75}Ga_{0.25}Se_2$ films

Structural

The precursor powder is used for screen printing followed by annealing at five different temperatures from 300 to 400 °C. Deposited films are found to exhibit (112), (220)/(204), and (312)/(116) reflections corresponding to chalcopyrite structure of $CuIn_{0.75}Ga_{0.25}Se_2$ as shown in Fig. 4a, without any preferred orientation peak, which is confirmed by the nearly equal texture coefficient calculated from Eq. 3 and given in Table 4. It has been reported that in the case of chalcopyrite $CuIn_xGa_{1-x}Se_2$ thin films strongest reflexions are the (112) and the overlapping (220)/(204), which corresponds to different preferred orientations (Olejnícek et al. 2010).

Micro structural parameters such as grain size (D), dislocation density (δ), and strain (ε) of the deposited films have been determined by the relations (1, 4, and 5) and given in Table 5.

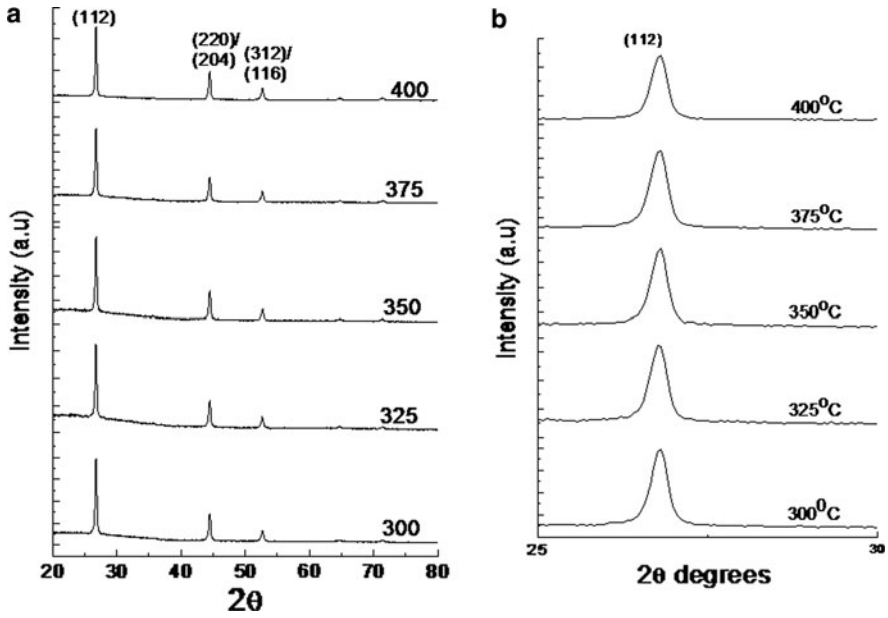

Fig. 4 **a** XRD pattern of screen printed $CuIn_{0.75}Ga_{0.25}Se_2$ films. **b** Zoom in image which shows left shift in peak

Table 4 Calculated texture coefficients of screen printed $CuIn_{0.75}Ga_{0.25}Se_2$ films

(*hkl*): Annealing temp (°C)	(112)	(220)/(204)	(312)/(116)
300	1.232	1.066	0.702
325	1.128	0.970	0.900
350	1.124	1.038	0.837
375	1.160	1.048	0.792
400	1.121	1.063	0.815

Table 5 Structural parameters of screen printed $CuIn_{0.75}Ga_{0.25}Se_2$ films

Annealing temp (°C)	Grain size D (nm)	Strain $\varepsilon \times 10^{-3}$	Dislocation density $\delta \times 10^{15}$
300	43.9	4.76	5.197
325	43.6	4.81	5.254
350	43.4	4.86	5.310
375	42.1	4.98	5.636
400	42.4	4.93	5.575

$$\beta = [\lambda/(D\cos\theta)] - \varepsilon\tan\theta \quad (4)$$

$$\delta = 1/D^2 \quad (5)$$

It is observed that grain size increases slightly for films compared to the precursor powder due to heat treatment. Dislocation density and strain values also remain almost the same irrespective of annealing temperature. Peak shift to lower angles in XRD patterns without remarkable growth of particles has been noticed as given in Fig. 4b. In general, XRD peak shift of $CuIn_xGa_{1-x}Se_2$ is considered to be related to the Ga contents in film, where as Ga contents increase the lattice constant decreases and subsequently diffraction angle increases (Ahn et al. 2008). Thus, peak shift appearing in Fig. 4b with heat treatment temperatures can be attributed to decrease of Ga content in films. To determine the change in Ga

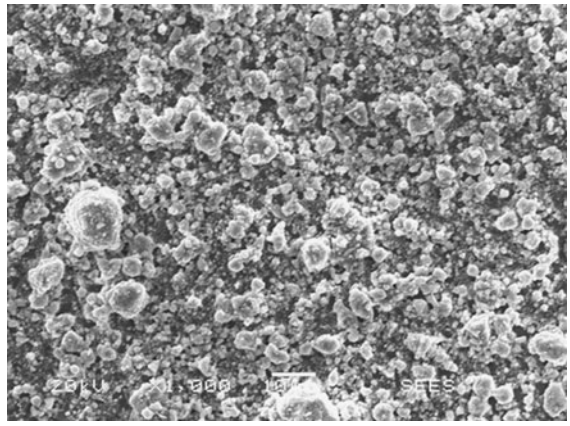

Fig. 5 SEM image of screen printed $CuIn_{0.75}Ga_{0.25}Se_2$ films annealed at 400 °C and the precursor material

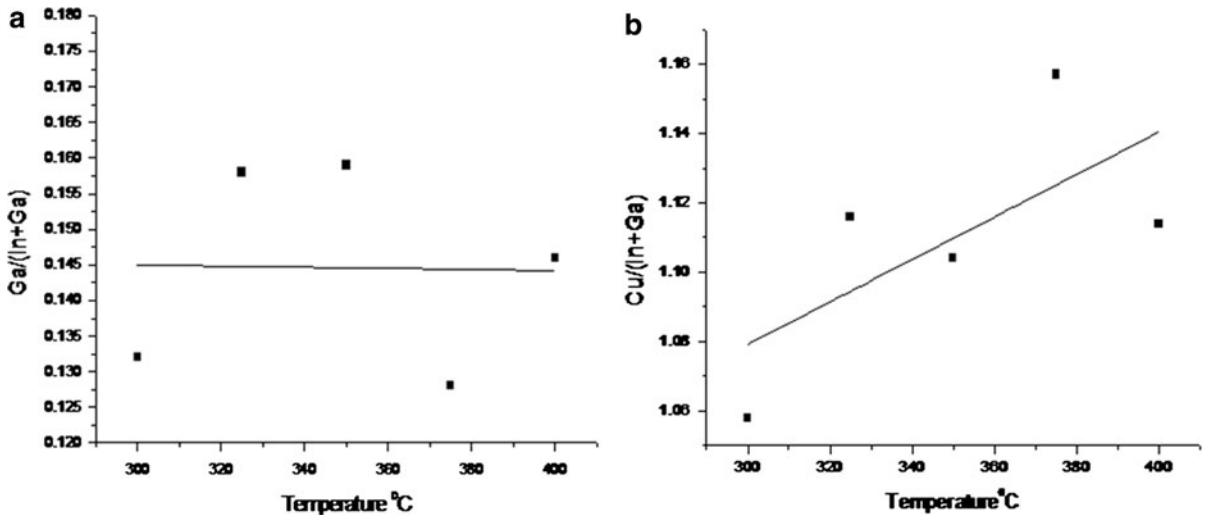

Fig. 6 **a** Ga/(In + Ga) versus annealing temperature, **b** Cu/(In + Ga) versus annealing temperature

content, EDX composition analysis has been carried out, and the results are discussed below.

Morphology and composition

SEM image given in Fig. 5, shows the presence of smaller particles, which is in agreement with XRD results. (Ahn et al. 2007) have reported that increase in temperature to 500 °C leads to the formation of impure binary phases due to loss of Ga. This is very well observed from EDX composition analysis of film where the ratio of Ga/(In + Ga) and Cu/(In + Ga) has been plotted in Fig. 6a and b, respectively. It is observed that higher the heat treatment temperature was, lower were the Ga contents in films, which is consistent with XRD data in Fig. 5a as stated above. Ratio of Ga/(In + Ga) was found to be almost independent of temperature, reflecting that the In contents in films decreased together with Ga keeping the Ga/(In + Ga) ratio of particles constant. Accordingly, simultaneous decrease in Ga and In contents resulted in the increase in Cu/(In + Ga) with increase in temperature as given in Fig. 6b. Possible reasons for this enhanced In and Ga loss are that the nanosized particles generally have large surface energies, meaning that they are thermodynamically unstable and the vapor pressures of constituents of the particles are notably higher than those of bulk materials (Suryanarayana et al. 2001), resulting in significant reduction of evolution temperature of gas phases. Other explanations include the poor crystallinity of nanoparticles used (Ahn et al. 2008) and no Se supply during the heat treatment at all. Apart from this there were no traces of other impurities as shown in Fig. 7, composition mapping of screen printed CIGS films. Hence, confirming the purity of deposited films.

Conclusions

Single phase CIGS nanoparticles can be prepared by ball milling for more than 45 min at 1200 rpm. Shift in XRD peaks toward lower angle is observed due to stress induced during the process of milling. HRTEM analysis confirmed the nanoparticle size of 11.73 nm which was in agreement with the value calculated by Scherrer's formula. Numerous dislocations and distortions were induced during milling leading to the formation of nanoparticles. Composition analysis revealed a slight deviation in the milled samples from the initial composition due to low volatilization of Se. Heat treatment of screen printed $CuIn_{0.75}Ga_{0.25}Se_2$ films in nitrogen atmosphere induced loss of In and Ga contents due to thermodynamic instability of nanoparticles. Therefore, we conclude that either it be milled precursor nanoparticles or nanoparticle films, the exact reproducibility of composition always has some hindrances such as low volatilization of Se and thermodynamically unstable nature of nanoparticles.

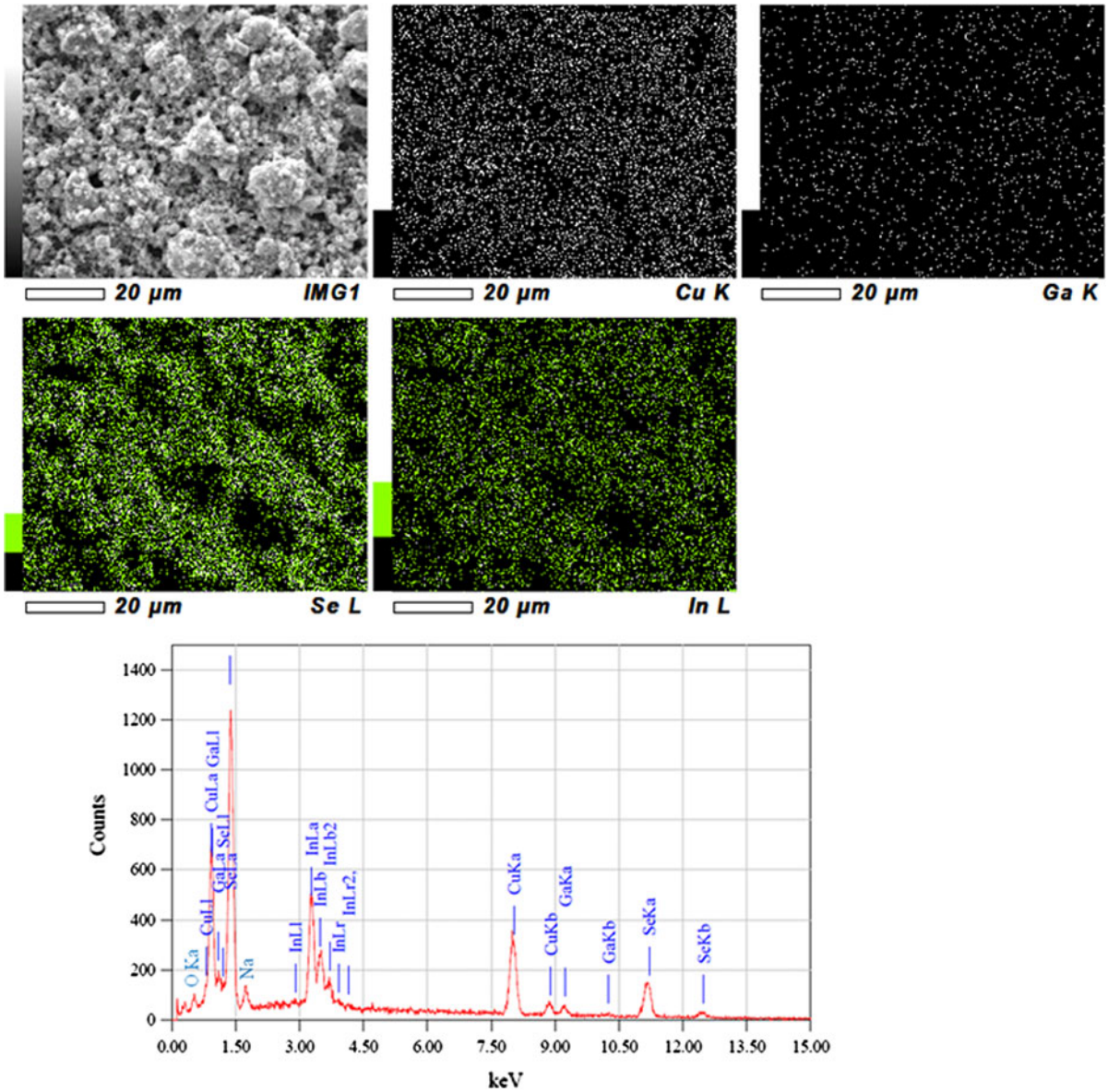

Fig. 7 Composition mapping analysis of screen printed $CuIn_{0.75}Ga_{0.25}Se_2$ film annealed at 400 °C

Acknowledgments The authors would like to acknowledge Dr. Hector Calderón and his team of Escuela Superior de Fisica y Matematicas del IPN for providing the ball mill for sample preparation. We acknowledge the Solid State Physics group, Department of Physics, CINVESTAV for the XRD measurement. We acknowledge Luis Rendón from IFUNAM for his technical help in HRTEM. We also acknowledge the contribution of Dr. Gaspar Casados-Cruz for making the SEM-EDX measurements. One of the authors B. Vidhya is thankful for the scholarship provided by CONACYT to pursue the Doctorate program.

References

Ahn SJ, Kim KH, Chun YG, Yoon KH (2007) Nucleation and growth of Cu(In, Ga)Se_2 nanoparticles in low temperature colloidal process. Thin Solid Films 515:4036–4040

Ahn SJ, Kim KH, Yoon KH (2008) Nanoparticle derived Cu (In, Ga) Se_2 absorber layer for thin film solar cells. Colloids Surf A Physicochem Eng Asp 313–314:171–174

Benslim N, Mehdaoui S, Aissaoui O, Benabdeslem M, Bouasla A, Bechiri L, Otmani A, Portier X (2010) XRD and TEM

characterizations of the mechanically alloyed $CuIn_{0.5}Ga_{0.5}Se_2$ powders. J Alloys Compd 489:437–440

Cai S, Tsuzuki T, Fisher TA, Nener BD, Dell JM, McCormick PG (2002) Mechanochemical synthesis and characterization of GaN nanocrystals. J Nanopart Res 4:37–367

Chityuttakan C, Chinvetkitvanich P, Yoodee K, Chatraphorn S (2006) In situ monitoring of the growth of Cu(In, Ga)Se_2 thin films. Sol Energy Mater Sol Cells 90:3124–3129

Choi IH, Lee DH (2007) Preparation of $CuIn_{1-x}Ga_xSe_2$ films by metalorganic chemical vapor deposition using three precursors. Thin Solid Films 515(11):4778–4782

Chun YG, Kim KH, Yoon KH (2005) Synthesis of $CuInGaSe_2$ nanoparticles by solvothermal route. Thin Solid Films 480–481:46–49

Contreras MA, Ramanathan K, Abushama J, Hasoon F, Young DL, Egaas B, Noufi R (2005) Diode characteristics in state-of-the-art ZnO/CdS/Cu($In_{1-x}Ga_x$)Se_2 solar cells. Prog Photovolt Res Appl 13:209–216

Contreras MA, Romero MJ, Noufi R (2006) Characterization of Cu(In, Ga)Se_2 materials used in record performance solar cells. Thin Solid Films 511–512:51–54

Djekoun A, Bouzabata B, Otmani A, Greneche JM (2006) X-ray diffraction and Mössbauer studies of nanocrystalline Fe–Ni alloys prepared by mechanical alloying. Catal Today 113:235–239

Dodd A, McKinley A, Tsuzuki T, Saunders M (2008) A comparative evaluation of the photocatalytic and optical properties of nanoparticulate ZnO synthesised by mechanochemical processing. J Nanopart Res 10(Suppl 1): 243–248

Gesenhues U (1999) Substructure of titanium dioxide agglomerates from dry ball-milling experiments. J Nanopart Res 1:223–234

Gmelin E, Hönle W (1995) Anomalous lattice specific-heat of $LiInSe_2$ at low-temperatures. Thermochim Acta 269–270: 575–590

Jäger-Waldau A, Meyer N, Weiss T, Fiechter S, Lux-Steiner MCh, Tempelhoff K, Richter W (1998) A new approach to grow polycrystalline $CuGaSe_2$ thin films: chemical vapor deposition with I2 as transport agent. Jpn J Appl Phys 37:1617–1621

Kaufamn CA, Neisser A, Klenk R, Scheer R (2005) Transfer of Cu(In, Ga)Se_2 thin film solar cells to flexible substrates using an in situ process control. Thin Solid Films 480–481:515–519

Lin Y, Chen Y, Feng M, Yan A, Zhuang X (2008) One-pot synthesis of soluble nanoscale CIGS photoactive functional materials. Nanoscale Res Lett 3:21–24

Lundberg LuJ, Rockett A, Edoff M, Stolt L (2003) Diffusion of indium and gallium in Cu(In, Ga)Se_2 thin film solar cells. J Phys Chem Solids 64:1499–1504

Luo P, Yu P, Zuo R, Jin J, Ding Y, Song J, Chen Y (2010a) The preparation of $CuInSe_2$ films by solvothermal route and non-vacuum spin-coating process. Physica B 405: 3294–3298

Luo P, Zuo R, Chen L (2010b) The preparation of $CuInSe_2$ films by combustion method and non-vacuum spin-coating process. Sol Energy Mater Sol Cells 94:1146–1151

Nouiri M, Ben Ayadi Z, Khirouni K, Alaya S, Djessas K, Yapi S (2007) Effect of substrate temperature and source grain size on the structural and electrical properties of CSVT grown Cu($In_{1-x}Ga_x$)Se_2 thin films. Mater Sci Eng C 27:1002–1006

Olejníček J, Kamler CA, Mirasano A, Martinez-Skinner AL, Ingersoll MA, Exstrom CL, Darveau SA, Huguenin-Love JA, Diaz M, Ianno NJ, Soukup RJ (2010) A non-vacuum process for preparing nanocrystalline $CuIn_{1-x}Ga_xSe_2$ materials involving an open-air solvothermal reaction. Sol Energy Mater Sol Cells 94:8–11

Panthani MG, Akhavan V, Goodfellow B, Schmidtke JP, Dunn L, Dodabalapur A, Barbara PF, Korgel BA (2008) Synthesis of $CuInS_2$, $CuInSe_2$, and Cu(In_xGa_{1-x})Se_2 (CIGS) nanocrystal "inks" for printable photovoltaics. J Am Chem Soc 130(49):16770–16777

Reddy BSB, Rajasekhar K, Venu M, Dilip JJS, Das Siddhartha, Das Karabi (2008) Mechanical activation-assisted solid-state combustion synthesis of in situ aluminum matrix hybrid (Al_3Ni/Al_2O_3) nanocomposites. J Alloys Compd 465:97–105

Sakurai K, Hunger R, Tsuchimochi N, Baba T, Matsubara K, Fons P, Yamada A, Kojima T, Deguchi T, Nakanishi H, Niki S (2003) Properties of $CuInGaSe_2$ solar cells based upon an improved three-stage process. Thin Solid Films 431–432:6–10

Shen J, Kim WK, Shang S, Chu M, Cao S, Anderson TJ (2006) Thermodynamic description of the ternary compounds in the Cu–In–Se system. Rare Met 25:481

Sherif El-Eskandarany M, Saida J, Inoue A (2003) Mechanically induced solid-state devitrifications of $Zr_{70}Pd_{20}Ni_{10}$ glassy alloy powders. Metall Mater Trans A 34A:893

Suri D, Nagpal K, Chadha G (1989) X-ray study of $CuGa_xIn_{1-x}Se_2$ solid solutions. J Appl Crystallogr 22:578

Suryanarayana C, Yoo SH, Groza JR (2001) Consolidation of mechanically alloyed Cu–In–Ga–Se powders. J Mater Sci Lett 20:2179–2181

Vidhya B, Velumani S, Arenas-Alatorre JesusA, Morales-Acevedo Arturo, Asomoza R, Chavez-Carvayar JA (2010) Structural studies of mechano-chemically synthesized $CuIn_{1-x}Ga_xSe_2$ nanoparticles. Mater Sci Eng B 174:216–221

Virtuani A, Lotter E, Powallia M (2006) Influence of Cu content on electronic transport and shunting behavior of Cu(In, Ga)Se_2 solar cells. J Appl Phys 99:014906

Wada T, Kinoshita H (2005) Rapid exothermic synthesis of chalcopyrite-type $CuInSe_2$. J Phys Chem Solids 66:1987–1989

Wu S, Xue Y, Zhang Z (2010) Microanalysis on $CuInSe_2$ compound synthesized by mechanochemical processing. J Alloys Compd 491:456–459

Yang H, Qiu GZ, Zhang XC, Tang A, Yang W (2004) Preparation of CdO nanoparticles by mechanochemical reaction. J Nanopart Res 6:539–542